

Document downloaded from:

<http://hdl.handle.net/10251/179753>

This paper must be cited as:

Uriarte, JA.; Damas Molla, L.; Sagarna, M.; Aranburu, A.; García García, F.; Antigüedad, I.; Morales, T. (2020). Characterization of complex groundwater flows in the environment of singular buildings by combining hydrogeological and non-destructive geophysical (ground-penetrating radar) techniques: Punta Begona Galleries (Getxo, Spain). *Hydrological Processes*. 34(4):1004-1015. <https://doi.org/10.1002/hyp.13635>



The final publication is available at

<https://doi.org/10.1002/hyp.13635>

Copyright John Wiley & Sons

Additional Information

Morales Tomas (Orcid ID: 0000-0002-6113-9677)

Characterization of complex groundwater flows in the environment of singular buildings by combining hydrogeological and non-destructive geophysical (ground-penetrating radar) techniques: Punta Begoña Galleries (Getxo, Spain)

Jesus A. Uriarte¹, Laura Damas Mollá¹, Maialen Sagarna², Arantza Aranburu³, Francisco García⁴, Iñaki Antigüedad¹, Tomás Morales^{1*}

¹Department of Geodynamics, Science and Technology Faculty, University of the Basque Country UPV/EHU, B° Sarriena s/n, E-48940 Leioa, Spain

²Department of Architecture, Faculty of Engineering, University of the Basque Country UPV/EHU, Plaza Europa 1, E-20018 Donostia, Spain

³Department of Mineralogy and Petrology, Science and Technology Faculty, University of the Basque Country UPV/EHU, B° Sarriena s/n, E-48940 Leioa, Spain

⁴Department of Cartographic Engineering, Geodesy and Photogrammetry, Polytechnic University of Valencia, Camino de Vera s/n, E-46022 Valencia, Spain

* Corresponding author: tomas.morales@ehu.eus

Abstract

Locating and quantifying groundwater flow in many built-up areas is a priority with regard to their complete restoration. In this work, a hydrogeological survey of the surroundings of the

This article has been accepted for publication and undergone full peer review but has not been through the copyediting, typesetting, pagination and proofreading process which may lead to differences between this version and the Version of Record. Please cite this article as doi: 10.1002/hyp.13635

Punta Begoña Galleries (Getxo, Bizkaia), built on a coastal cliff, was completed by using ground penetrating radar (GPR) testing. Thus, the preliminary characterization of soils and rocks in accessible areas of the cliff was first improved by hydrogeological information gathered from a single survey borehole, including permeability measurements by low pressure injection tests (LPTs) and continuous water level monitoring. As a complementary method, the non-destructive GPR technique was performed during both dry and wet hydrological periods and in tandem with the injection tests, providing more complete spatial and temporal images of water flows. Specifically, GPR allows mapping of flow paths in soils and assessing the continuity of fractures in rock masses. Altogether, this complementary approach provides greater knowledge of complex underground flow dynamics in built environments, thus making it easier to make decisions for their management.

Keywords

Complex water flow, hydrogeological survey, ground penetrating radar, heritage

1. Introduction

Precise characterization of preferential flow paths in heterogeneous soils and fractured rock massifs remains one of the most important challenges for applied hydrology. In our work, the identification of underground flows in the vicinity of a "historic building", dilapidated after years of neglect, was addressed by means of a direct characterization of foundation materials on the cliff where the building was constructed and deepened by the hydrogeological information gathered from an exploratory borehole and completed by profiles developed using ground penetrating radar (GPR). The building in question: "Las Galerías Punta Begoña" (Getxo, Bizkaia) was built in the early 20th century. Its construction was carried out directly on a flyschoid cliff, using innovative construction materials for those times such as reinforced concrete. After years of neglect, in 2014, the Getxo Town Council, in agreement with the University of the Basque Country, promoted a project to recover and enhance the Galleries.

The main conservation problems affecting both the materials and the structure were related to direct precipitation and to surface and groundwater flows. For the first case, a project was

implemented to waterproof the roofs of the building. In the second case, prior to the drainage system project, it was essential to know the particularities of flow in the soils and in the fractured rocky environment.

In this context, to identify and characterize the local underground flow systems affecting the Punta Begoña building, a threefold research strategy was undertaken. On the one hand, a preliminary survey of the accessible areas of the cliff was carried out to identify the different materials that made up the building environment. This information was enhanced by hydrogeological records obtained from a survey borehole in which 6 water injection tests were carried out at different depths. Thus, direct measurements of the permeabilities at different ground levels were obtained (Price, Robertson, & Foster, 1977; Ford & Williams, 1989; Nappi, Esposito, Piscopo, & Rega, 2005; Sánchez, Foyo, & Tomillo, 2006). In Punta Begoña, to limit the development of hydraulic fracking processes in the fractured medium, the injection tests were carried out in accordance with the low pressure test (LPT) methodology (Sánchez, Foyo, & Tomillo, 2006; Angulo, Morales, Uriarte, & Antigüedad, 2011). In any case, this is an invasive technique of limited use in areas such as that studied here. Therefore, to complement this information and to obtain a broader view of the flow scheme, the previous information was complemented by using GPR. This high-frequency electromagnetic technique (25 MHz–2 GHz) is currently an important geophysical tool for investigating the shallow subsurface (Forte & Pipan, 2017) and provides significant resolution and excellent sensitivity to variations in pore fluid content and lithology (Davis & Annan, 1989, Huisman, Hubbard, Redman, & Annan, 2003, Huisman, Snepvangers, Bouten, & Heuvelink, 2003). Over the past decades, GPR has been employed to resolve various geological and engineering issues, including, among others, soil water content measures (van Overmeeren, Sariowan, & Gehrels, 1997; Weiler, Steenhuis, Boll, & Kung, 1998; Grote, Anger, Kelly, Hubbard, & Rubin, 2010; Huisman, Sperl, Bouten, & Verstraten, 2001; Huisman & Bouten, 2003, Galagedara, Parkin, & Redman, 2003), soil moisture mapping at the field scale (Weihermüller, Huisman, Lambot, Herbst, & Vereecken, 2007, Grote, Hubbard, & Rubin, 2003, Minet, Bogaert, Vanclooster, & Lambot, 2012), and identification of near-surface structures and seepage paths (Birken & Versteeg, 2000; Trinks, Wachsmuth, & Stümpel, 2004; Neal, 2004; Klenk, Jaumann, & Roth, 2015; Su, Xu, Geng, & Liang, 2017). Regarding the application of GPR in rock massifs, its main uses are related to the identification of major discontinuities and fractures, particularly in karst environments (Grandjean & Gourry, 1996; Chamberlain, Sellers, Proctor, & Coard, 2000; Pueyo Anchuela, Casas-Sainz, Soriano, & Pocoví-Juan, 2009; Deparis, Garambois, & Hantz, 2007; Garcia-

Garcia, Valls-Ayuso, Benlloch-Marco, & Valcuende-Paya, 2017); for less clear features and structures, the contrast of GPR images along with direct observations allows calibration and validation of the results (Longoni et al., 2012; Fernandes, Medeiros, Bezerra, Oliveira, Cazarin, 2015; Pipan, Forte, Guangyou, & Finetti, 2003).

Thus, this study aims to evaluate the use of hydrogeological and geophysical techniques in a complementary manner for the recognition of complex flow dynamics in sensitive built environments. In this way, the information obtained from direct observations and from a single survey borehole was expanded by using non-destructive georadar (GPR) techniques that are of particular interest for applications in sensitive environments, where drilling is inadvisable or even undesirable (van Overmeeren, 1994).

2. Study framework: geographic and hydrogeological context

The Punta Begoña Galleries are located in the municipality of Getxo, on the cliffs that characterize the Basque coast in the Bay of Biscay (Fig. 1). They were projected by Ricardo Bastida as an extension of Horacio Etxebarrieta's house, now disappeared. The latter was one of the most important entrepreneurs in Bizkaia during the nineteenth to the twentieth century. The privileged location of the built complex, in a watchtower located at the entrance of the Bilbao Estuary, allowed him to live in a healthy environment from which to contemplate and monitor mining activity on the opposite hillsides, as well as the entry and exit of boats in the port of Bilbao.

From a geological point of view, materials cropping out in this sector of the coast are thick Mesozoic and Cenozoic successions of the Alpine cycle (EVE, 1993). The general configuration of these materials shows a northwest-southeast direction that steeply dips toward the south. In the area where the galleries were built, materials show a flyschoid type of alternation, consisting of hemipelagic marls and marly limestones (Upper Cretaceous grey and red marls and marly limestones, Fig. 1). Toward the north, the newest materials forming the Cenozoic series begin with Danian pink and grey limestones and calcareous marly limestones and continue with predominantly terrigenous sediments, with sandstones of different compositions.

From a hydrogeological point of view, the materials in this sector do not constitute aquifers with continuous groundwater levels as such, except for the valley bottom Quaternary sediments. Regarding the consolidated geological materials mentioned previously, their dominantly marly nature causes their overall permeability to be low. In any case, the occasional presence of more carbonate-rich or sandy levels, and particularly the development of secondary porosity features aligned congruent to the bedding, e.g., bed partings, or related to systematic and non-systematic fractures (Bloomfield, 1996; Graham Wall, 2006; Fan, Toran & Schlische, 2007; Worthington, 2015; Runkel et al., 2018) result in local flows determining the movement of underground waters.

In this context, the Punta Begoña Galleries were built directly on the cliff face at the beginning of the 20th century, and their construction coincided with the beginning of the use of reinforced concrete (Rosell & Cárcamo, 1994; Díaz Morlán, 1999, 2011). The building is structured as two main facades, separated by a semi-circular structure that acts as a junction: the so-called southwest gallery (SWG), with a wide corridor; and the northwest gallery (NWG), with an elevated corridor and the largest room known as the hall (Fig. 2). It is precisely in this space where the main damage caused by water entry and humidity has occurred and where the research work was focused.

3. Methodology

3.1. Preliminary geological investigation

Geological and geomechanical analyses were performed in openings behind the building from which the original cliff outcrops were accessible. From these outcrops, it was possible to make a first determination of the materials and to obtain the basic parameters that characterized the fracture network from a hydrogeological point of view (Berkowitz, 2002). These characterizations involved mechanical joints and bed parallel partings (Runkel et al., 2018). With this aim, conventional geological mapping was carried out. The mapping included quantitative information (Hoek & Bray, 1981; Priest, 1993; Bloomfield, 1996) on the number, orientation, spacing, aperture, persistence and filling of the more significant features and fracture sets. Orientations were determined through the use of a compass and were plotted on a stereogram, allowing identification of the orientations of the bed partings (Bp) and the main joint sets (namely, Jn).

3.2. Borehole testing and injection tests

To broaden the information regarding the building surroundings, 1 survey borehole was drilled at the top of the cliff. This borehole, with a depth of 25 m and an inclination of 25° toward the building, was drilled with continuous core recovery. It allowed determination of the materials traversed and, in the case of the rock massif, observations of the layout and the in-depth characteristics of the fracture network.

This borehole was utilized to obtain quantitative information on rock mass permeabilities by conducting six constant-pressure injection tests. To minimize the possible effects of hydraulic fracturing, the injection tests were carried out in 3-m sections that were isolated between expandable double packers, according to the low-pressure test (LPT) methodology (Sánchez et al., 2006, Angulo et al., 2011). Thus, the sequence of pressure levels consisted of 0-1-2-3-5-3-2-1 gauge pressures in bars, and the duration of each pressure step was 5 min, after stabilization. Here, the steady-state flow was governed by the Laplace equation:

$$\frac{1}{r} \frac{\partial}{\partial r} \left(\frac{1}{r} \frac{\partial u}{\partial r} \right) + \left(\frac{\partial^2 u}{\partial z^2} \right) = 0 \quad (1)$$

where u is the pressure of the pores and is represented in cylindrical coordinates (r, z).

Equation (1) does not have an analytic solution. For ratios of L/r_w greater than 10, the usual equation for calculating the hydraulic conductivity, that assumes semi-ellipsoidal equipotential surfaces and symmetrical flow lines with respect to a horizontal plane that goes through the midpoint of the cylindrical end, is (Sánchez et al., 2006; Department of the Interior Bureau of Reclamation, 1998; Sudo et al., 2004, Hamma et al., 2007):

$$k = \frac{Q \ln(L/r_w)}{2\pi L H_0} \quad (2)$$

where Q is the flow rate, r_w is the radius of the borehole, L is the test section, and H_0 is the water head difference.

It should be noted that these pressure injection tests favour a greater presence of water in the functional fracture network of the medium. Finally, the borehole was instrumented with a probe

that continuously recorded conductivity, temperature and pressure/depth (CTD-diver) and was placed at a depth of 21.15 m, according to the drilling axis.

3.3. GPR method

The GPR technique consists of the propagation of short electromagnetic pulses ($t \leq 1$ ns) in the studied medium. Reflection of these pulses occurs when sharp changes exist in the electromagnetic properties of the medium: magnetic permittivity, electrical conductivity and dielectric permittivity. In GPR records, an electromagnetic pulse is characterized by the velocity, frequency content and amplitude of the wave. Consequently, these characteristics of the GPR signal are greatly influenced by the electromagnetic properties of the medium. The contributions of electrical conductivity and magnetic permeability to the recorded signal cannot be distinguished in typical GPR studies using frequencies between 8 MHz and 2.5 GHz (Schmalholz, Stoffregen, Kemna, & Yaramanci, 2004; Pérez-Gracia, García, & Rodríguez Abad, 2008). In low-loss media, the dielectric permittivity (ϵ_r) can be calculated approximately according to the equation:

$$\epsilon_r = \left(\frac{c}{v}\right)^2 = \left(\frac{ct}{2h}\right)^2 \quad (3)$$

where h is the layer depth, t is the two-way travel time (elapsed time) in the GPR profile, and c is the speed of light (0.299 m/ns) (Conyers, 2013; Pérez, 2001).

Average velocities are obtained from (Conyers, 2013; Pérez, 2001):

$$v = \frac{2h}{t} \quad (4)$$

The amplitudes of the reflections generated at the interfaces between two materials can be calculated using the reflection coefficients (R) (Conyers, 2013). The amplitudes and reflection strengths of GPR signals are proportional to the contrasts in the dielectric permittivities across the reflector boundaries and are a function of the reflection coefficients. In low-loss media (non-magnetic media), an adequate approximation for the expression of the reflection coefficients in most GPR studies is given by (Neal, 2004):

$$R = \frac{\sqrt{\epsilon_{r1}} - \sqrt{\epsilon_{r2}}}{\sqrt{\epsilon_{r1}} + \sqrt{\epsilon_{r2}}} \quad (5)$$

where ϵ_{r1} is the dielectric permittivity of the upper layer and ϵ_{r2} is the dielectric permittivity of the lower layer. From this expression, it can be deduced that, the greater the difference between the electromagnetic parameters of the media, the greater is the reflection coefficient. That is, the greater the contrast between the two media that are in contact, the greater is the percentage of incident energy that will be reflected at the reflector boundary/discontinuity. Therefore, the highest amplitude radar reflections will take place mainly at the interfaces of two geological materials that have considerably different electromagnetic properties (Pérez-Gracia et al., 2008; Lunt, Hubbard, & Rubin, 2005).

For the case where the water content in a medium is significant, this water content becomes an influential factor for the values of the dielectric permittivities of geological materials since the dielectric permittivity of water (81) is much greater than that of any other geological material (3-40). According to expression (5), high amplitude radar reflections are also generated at the interfaces of water-affected (wetter) areas in the subsoil and any surrounding lower-velocity geological materials. So, for this study, in the GPR records, these high-amplitude radar reflections corresponded to the water-affected (wetter) areas in the subsoil (Longoni et al., 2012, Pérez-Gracia et al., 2008, Lunt et al., 2005).

In agreement with previous studies, particularly those aimed at the identification of fractures in healthy rocks and their comparisons with observations of outcrops (Longoni et al., 2012; Fernandes et al., 2015), in this study, a 200 MHz centre-band frequency antenna with a time window of 200 ns was used. In addition, a 400 MHz centre-band frequency antenna with a time interval of 80 ns was used to improve resolution at the expense of decreased wave penetration (Davis & Annan, 1989). Data collection was carried out over a total of 14 profiles: 9 profiles on the cliff top (8 profiles spaced every 6 m and 1 orthogonal profile); 3 profiles inside the hall, spaced 6 m and oriented perpendicular to the cliff; and 2 profiles in the space under the hall (Fig. 3).

Since the water content influences the electromagnetic response (Garcia-Garcia et al., 2017; Pérez-Gracia et al., 2008; Lunt et al., 2005), two GPR data acquisition surveys were carried out on the cliff top for two different hydrodynamic periods: a period of intense rains and a dry

period. Radar reflections (profiles 41 to 49) were correlated with the stratigraphy derived from field observations and from borehole testing. This correlation was used for time-depth conversion of the acquired radar datasets. The respective average velocities in the interpretations relative to the depths (ground truthing method) (Benedetto, Tosti, Bianchini Ciampoli, & D'Amico, 2017; Conyers & Lucius, 1996) were calculated using equation (4). These velocity estimates for each dataset should be considered as acceptable given the inherent imprecision of the GPR technique (Conyers, 2013, Conyers & Lucius, 1996).

In addition, part of the survey (profiles 85 to 89) was carried out concurrently with the injection tests to take advantage of the increased water presence in the rock mass fractures. This allowed improvements in the accuracy rates for recording fractures within the sound rock in the GPR records, as the dielectric contrast values at the fracture boundaries and the amount of reflected energy from them augmented each other (Davis & Annan, 1989; Huisman et al., 2003; Longoni et al., 2012; Pérez-Gracia et al., 2008, Lunt et al., 2005). So, the respective reflection coefficients (equation 5) also increased. This increase in the values of the reflection coefficients allowed the detection of hydraulically active fractures in the recordings in a clearer and more effective way. The periods of water injection were also used to conduct 2 transverse profiles (88 and 89) in the fill underneath the hall.

Post-acquisition processing procedures were necessary for application to the raw field GPR datasets (Conyers, 2013; Benedetto et al., 2017). In this study, a data processing procedure was applied to the raw radar datasets using RADAN software developed by Geophysical Survey Systems, Inc. (GSSI). First, 1D processing was applied consisting of a zero-time correction (time-zero adjustment) for removing the delay time from the first reflection. Next, 2D processing was applied to the reflection profiles as follows: (1) a background removal filter was applied for removing the average values across all traces on the horizontal axis (horizontal banding); (2) band-pass filters using the centre frequencies of the 200 MHz and 400 MHz antennae were used and were applied to remove both low and high frequency noise in the vertical and horizontal directions; (3) a linear amplitude gain was applied to compensate for the amplitude reductions due to the filters used; (4) a Kirchhoff migration filter was applied to the profiles using the calculated average velocities for each dataset for removing diffracted reflections of radar energy and to move dipping reflectors to their true subsurface positions. Finally, a time to depth conversion was performed using the calculated average velocities. The 3D processing was applied as follows: each processed reflector profile was aligned within a

grid to produce horizontal amplitude maps. Some amplitude depth-slice maps were created at different levels for mapping the subsurface. Amplitude depth-slice maps from the 3D model were used to identify flow patterns at constant depths. The resulting depth-slice amplitude maps from the 3D model allowed pinpointing the evidence for flow paths in the studied subsurface volume (Pérez, 2001; Leckebusch, 2003).

4. Results

4.1. Differentiation of materials

First, the recognition of materials from direct observations and borehole testing made it possible to distinguish 3 main units:

1) A surface unit formed by topsoil, anthropogenic fill and altered rock. This unit reaches thicknesses of 1 to 2.4 m and is located in the upper terrace of the building.

2) Below the previous level is a rock massif made up of grey marls and marly limestones on which the building was constructed. A change to reddish marls at a depth of 23.40 m was recorded in the borehole. In the detailed cartography carried out in the accessible spaces of the cliff, it was possible to differentiate more marly and more clayey sections, whose different competition generates changes in the original cliff relief (Fig. 4).

The characterization of the fracture network allowed the recognition of 3 main sets (Figs. 4 and 5; Table 1). Of these, the bed partings (B_p) are oriented perpendicular to the cliff and have an average spacing of 0.32 m and an average aperture of 0.25 to 0.5 mm (partly open according to Duncan & Christopher, 2004). The main joint set (J_1) has an orientation parallel to the slope, with an average dip of 30° toward the slope; its average spacing is 0.41 m, and it has a slightly larger general opening (from 0.5 to 2.5 mm), with maxima of up to 10 mm (moderately wide). This set was recognizable in the borehole, where some wide fractures with clayey filling and small oriented pebbles were also observed (10-50 mm, Fig. 6), indicative of drag-out in the aqueous media. This joint also marks the cliff morphology to a great extent. The third joint set (J_2) dips inward toward the massif and has an average spacing of 0.60 m and a small general opening (0.1 to 0.25 mm, tight).

Regarding the massif permeability, the LPTs provided hydraulic conductivity values ranging from a maximum of $2.30 \cdot 10^{-3}$ cm/s, in the most surficial tested section, to $1.24 \cdot 10^{-5}$ cm/s

in the deepest section (Fig. 6). According to the criteria of Sánchez et al. (2006), the massif would be permeable up to 18.12 m depth along the drilling axis, with hydraulic conductivity values greater than $6.76 \cdot 10^{-5}$ cm/s. The basal section has hydraulic conductivity values lower than $2.25 \cdot 10^{-5}$ cm/s, which, according to this author, marks the limit of the impervious materials and coincides with the solid rock that has no hydraulically active fractures. Finally, it should be noted that during the tests, the injection water flow was detected through the masonry wall that forms the base of the building, mainly through a joint between blocks at a height of 8.27 m.a.s.l.

3) Finally, in the space underneath the hall, there is a fill consisting of materials from excavations carried out during the construction and that were dumped into this space. This fill is therefore made up of heterogeneous fragments of the same materials outcropping on the cliff.

4.2. Groundwater flow dynamics

The results of the GPR study allowed better characterization and understanding of the dynamics of groundwater flow in the building environment.

In the upper terrace, the profiles carried out made it possible to analyse 2 well-differentiated hydrodynamic periods. The GPR records were correlated with the depths of materials observed in the borehole to obtain GPR wave velocities and the corresponding dielectric permittivity values. The light zones in the GPR records indicated higher amplitude signals and higher recorded energies. These zones were related to moist areas in the subsoil.

During the rainy season (Fig. 7a), an average GPR wave velocity of 0.082 m/ns was calculated for the most surficial unit of materials, which corresponds to a dielectric permittivity of $\epsilon = 13.25$ (Equation 4). The medium showed a certain homogeneity, although there were 2 zones with relatively high amplitudes and with wave velocities of 0.072 m/ns ($\epsilon = 17.24$) and 0.065 m/ns ($\epsilon = 21.16$), respectively. An average GPR wave velocity of 0.089 m/ns ($\epsilon = 11.35$) was estimated for the rock massif materials. During the driest period, the average GPR wave velocity of the most surficial unit increased to 0.091 m/ns, with a dielectric constant of 10.56 (Fig. 7b). It was also observed that these 2 highest-amplitude reflection zones showed much lower amplitudes than during the rainy season. Also, their average wave velocities of 0.081 m/ns ($\epsilon = 13.63$) and 0.074 m/ns ($\epsilon = 16.33$) were higher than during the rainy season. An

average GPR wave velocity of 0.088 m/ns ($\epsilon = 11.52$) was calculated for the rock massif materials during this period.

Thus, in rainy periods, the building acts as a barrier to the flow and practically the entire field is highly saturated with water. As the ground dries up, the flow tends to be concentrated in two morphologies similar to furrows and/or areas of greater permeability that channels the water in the subsoil, while in the rest of the field, there is a clear generalized decrease in moisture content. The orientation of the two identified morphologies coincides with the stratification that would mark the underlying relief on which the surface unit is placed. The intersection of these two lines of preferential flow with the building corresponds to the most altered areas and to the highest humidities and water presence in the building.

From this surface level onward, part of the rainwater reaches the rock mass relatively quickly after the rains, as can be seen from the piezometric level records in the borehole (Fig. 8). The maximum recorded groundwater level reached a height of 11.42 m.a.s.l., which coincides with the upper level of the fill in the space under the hall. The subsequent descent of the water is also rapid to a height of 6.27 m.a.s.l. In this way, water flow in the upper part of the massif evolves under unsaturated conditions by its fracture network. The 3 GPR profiles carried out in the salon, that were obtained simultaneously with the water injections, made it possible to continue mapping the open fractures that were identified in the borehole toward the interior of the massif (Fig. 8).

Thus, the contrasts in the electromagnetic waves responses corresponding to solid rock and fractures with the water presence generated differences in the profiles that correspond to the main set of joints (J_1). The hydraulic continuity of these joints in the layered sedimentary medium is favoured by the relative homogeneity of the marls and marly materials and the absence of mechanical stratigraphic boundaries that would limit the continuity of these fractures (Cooke, Simo, Underwood, & Rijken, 2006; Chang, Shan, Zhang, Tang, & Ru, 2015). In any case, it should be noted that the borehole and the profiles were obtained parallel to the bedding, which may explain the lack of representation of bed parallel partings in the records. The GPR signals underwent strong attenuation from 4 to 6 m depth, in an environment of decreasing permeability.

During the water injections, 2 GPR profiles were carried out in the space under the hall, perpendicular to those carried out in the salon, to differentiate between morphologies of

different natures. In both profiles, several zones of high-amplitude reflections were observed (Fig. 8), with GPR wave velocity values in a range between 0.068 m/ns ($\epsilon = 19.33$) and 0.074 m/ns ($\epsilon = 16.33$). These elements responded to areas of higher humidity and water flow. In addition, an average GPR wave velocity of 0.079 m/ns ($\epsilon = 14.12$) was estimated for the fill. The GPR record for the P88 profile showed a more irregular base morphology for the fill, with a strikingly narrower and deeper development element (Fig. 9) that coincides with a marked fracture of the massif on the surface. In the GPR record of profile P89, closest to the supporting wall of the building (Fig. 9), the contact between the original relief of the cliff and the base of the present fill was inferred. It should be noted that in the lower surroundings of the V-shaped morphology drawn in the record, the main outlet of the injected water from the borehole was located at a joint between the blocks of the masonry wall that forms the base of the building. These last observations allowed us to recognize how the water entering from the upper field reaches, through the massif fracture network, the fill that occupies the base of the space under the hall. This rapid water movement, implying a net connection between the groundwater and surface waters through a secondary bedrock pore network, is in agreement with the observations of other authors for the shallowest part of fractured sedimentary rocks (e.g., Runkel et al., 2003; Runkel, Tipping, Alexander & Alexander, 2006; Green, Runkel, & Alexander, 2012).

In this manner and given the identified drainage context, two action options are planned: a drainage from the upper terrace, to prevent the entry of water at the source and that, conveniently redirected, can even be used for building uses and its surroundings; and a drainage action from the lower masonry wall, by means of inclined drains that reach the circulation zones of the massif and facilitate direct water evacuation toward the outside.

5. Discussion and conclusions

The combined use of geological-hydrogeological and ground penetrating radar (GPR) techniques allows to advance in the recognition of complex underground flow environments. Thus, outcrop and borehole observations allow the establishment of an initial conceptual framework of the study area and provide local permeability measurements. Within this framework, it is possible to recognize the different types of underground materials and to establish the hydrogeological units that condition and determine the development of groundwater flows.

In any case, this image presents as its main drawback, a limited spatial scope, particularly in constructed spaces that must be respectfully researched. At this point, using geophysical techniques such as GPR allows completing the acquisition of the necessary information. Since GPR is also a non-destructive technique, its application can be repeated under different hydrogeological conditions, which helps to complete and refine the hydrodynamic model. Moreover, given that hydrogeological injection tests facilitate water access in the most functional flow network, this can be used to improve recognition of the fractured massif from GPR records. In this sense, the entry of water into the most functional fractures increases the difference in the reflection coefficients between the fractures and the sound rock mass (Grandjean & Gourry, 1996) and generates greater contrasts in the corresponding reflection profiles (high-amplitude reflective zones) (Longoni et al., 2012; Fernandes et al., 2015; Pérez-Gracia et al., 2008; Lunt et al., 2005).

In our work, using this dual approach in the environment of the Punta Begoña Galleries has allowed us to identify two lines of preferential flow on the upper terrace of the site, which concentrate the water flow as the drainage evolves and gives rise to the two main water entry points for the building. As far as the rock massif is concerned, the geophysical profiles acquired in tandem with the injection tests made it possible to recognize the continuity of the fractures inside the massif, particularly J1. This network provides the medium with secondary permeability that reaches hydraulic conductivity values from $1.54 \cdot 10^{-3}$ cm/s to $2.3 \cdot 10^{-3}$, while decreasing with depth. In any case, although the presence of water marks the main features recorded in the radargrams, the uncertainties that arise in the interpretation of this information (Davis & Annan, 1989; Fernandes et al., 2015; Turesson, 2006; Neto & Medeiros, 2006) make it necessary to contrast the results with the geological-hydrogeological information obtained by the direct methods. Finally, in the space beneath the hall of the building, the most marked forms of flow develop in the lower fill and are delimited by a line that draws the original relief of the cliff in rocky material; in any case, the presence of some relatively narrow morphologies in the GPR records indicates somewhat deeper flows along planes of weakness and fractures in the massif. These two forms of circulation determine the final water outlets from the building through the lower masonry wall that forms its base.

The complementary use of geological-hydrogeological prospecting and ground penetrating radar (GPR) techniques improve the investigation of complex shallow groundwater flows in built environments. The individual limitations of each technique, namely, (i) insufficient

outcrops and limited penetration in direct field observations, (ii) use limitations and local information in the case of survey boreholes and (iii) interpretation uncertainties in the case of GPR, can be overcome with their joint application. Thus, this study indicates that adequately processed geophysical information, comparing features seen in outcrops and boreholes with the features observed in GPR records, can more completely and more precisely identify and characterize the near-surface structures and seepage path dynamics. In built-up areas, these results can be used as guidelines to guide projects for the implementation of groundwater drainage systems that favour the conservation of buildings.

Acknowledgements

This study was carried out by the UPV/EHU Research Group IT-1029/16 (Government of the Basque Country) in the framework of the project "Puesta en valor del inmueble histórico cultural Galerías Punta Begoña (Getxo, Bizkaia)" under the cooperation agreement between the University of the Basque Country (UPV/EHU) and the City Council of Getxo (OTRI2016-0738). Finally, we thank the reviewers and the editors of HYP for their constructive comments and suggestions, which helped to improve the manuscript significantly. Finally, we thank the reviewers and the editors of HYP for their constructive comments and suggestions, which helped to improve the manuscript significantly.

Data availability statement

The data that support the findings of this study are available from the corresponding author upon reasonable request.

References

Angulo, B., Morales, T., Uriarte, J.A., & Antigüedad, I. (2011). Hydraulic conductivity characterization of a karst recharge area using water injection tests and electrical resistivity logging. *Engineering Geology*, 117, 90-96. <https://doi.org/10.1016/j.enggeo.2010.10.008>

Benedetto, A., Tosti, F., Bianchini Ciampoli, L., & D'Amico, F. (2017). An overview of ground-penetrating radar signal processing techniques for road inspections. *Signal Processing*, 132, 201-209. <https://doi.org/10.1016/j.sigpro.2016.05.016>

Berkowitz, B. (2002). Characterizing flow and transport in fractured geological media: A review. *Advances in Water Resources*, 25, 861-884. [https://doi.org/10.1016/S0309-1708\(02\)00042-8](https://doi.org/10.1016/S0309-1708(02)00042-8)

Birken, R., & Versteeg, R. (2000). Use of four-dimensional ground penetrating radar and advanced visualization methods to determine subsurface fluid migration. *Journal of Applied Geophysics*, 43, 215-226. [https://doi.org/10.1016/S0926-9851\(99\)00060-9](https://doi.org/10.1016/S0926-9851(99)00060-9)

Bloomfield, J. (1996). Characterisation of hydrogeologically significant fracture distributions in the chalk: an example from the Upper Chalk of southern England. *Journal of Hydrology*, 184, 355-379. [https://doi.org/10.1016/0022-1694\(95\)02954-0](https://doi.org/10.1016/0022-1694(95)02954-0)

Chamberlain, A.T., Sellers, W., Proctor, C., & Coard, R. (2000). Cave detection in limestone using Ground Penetrating Radar. *Journal of Archaeological Science*, 27, 957-964. <https://doi.org/10.1006/jasc.1999.0525>

Chang, X., Shan, Y., Zhang, Z., Tang, C., & Ru, Z. (2015). Behavior of propagating fracture at bedding interface in layered rocks. *Engineering Geology*, 197, 33-41. <https://doi.org/10.1016/j.enggeo.2015.08.010>

Conyers, L.B. (2013). *Ground-penetrating radar for Archaeology* (3rd ed.). Lanham: AltaMira Press.

Conyers, L.B., & Lucius, J.E. (1996). Velocity analysis in archaeological ground-penetrating radar studies. *Archaeological Prospection*, 3, 312-333. [https://doi.org/10.1002/\(SICI\)1099-0763\(199603\)3:1<25::AID-ARP39>3.0.CO;2-U](https://doi.org/10.1002/(SICI)1099-0763(199603)3:1<25::AID-ARP39>3.0.CO;2-U)

Cooke, M.L, Simo, J.A, Underwood, C.A, & Rijken, P. (2006). Mechanical stratigraphic controls on fracture patterns within carbonates and implications for groundwater flow. *Sedimentary Geology*, 184, 225-239. <https://doi.org/10.1016/j.sedgeo.2005.11.004>

Davis, J.L., & Annan, A.P. (1989). Ground-penetrating radar for high-resolution mapping of soil and rock stratigraphy. *Geophysical Prospecting*, 37, 531-551. <https://doi.org/10.1111/j.1365-2478.1989.tb02221.x>

Deparis, J., Garambois, S., & Hantz, D. (2007). On the potential of Ground Penetrating Radar to help rock fall hazard assessment: A case study of a limestone slab, Gorges de la Bourne (French Alps). *Engineering Geology*, 94, 89-102. <https://doi.org/10.1016/j.enggeo.2007.07.005>

Department of the Interior Bureau of Reclamation (1998). *Earth Manual Part 1* (3rd ed.). Denver: US Government Printing Office.

Díaz Morlán, P. (1999). *Horacio Echevarrieta, 1870-1963: el capitalista republicano* (1st ed.). Madrid: LID Editorial Empresarial.

Díaz Morlán, P. (2011). *Horacio Echevarrieta, empresario republicano (Bilbainos Recuperados)*, Bilbao: Muelle de Uribitarte Editores.

Duncan, C.W., & Christopher W.M. (2004). *Rock slope engineering. Civil and Mining* (4th ed.). London and New York: Spon Press.

Ente Vasco de la Energía (1993). *Mapa geológico del País Vasco: 37-IV Getxo, E:1/25.000*. Bilbao: Ente Vasco de la Energía.

Fan, Y., Toran, L., & Schlische, R.W. (2007). Groundwater flow and groundwater-stream interaction in fractured and dipping sedimentary rocks: Insights from numerical models. *Water Resources Research*, 43, W01409. <https://doi:10.1029/2006WR004864>

Fernandes Jr. A.L., Medeiros, W.E., Bezerra, F.H.R., Oliveira Jr. J.G., & Cazarin, C.L. (2015). GPR investigation of karst guided by comparison with outcrop and unmanned aerial vehicle imagery. *Journal of Applied Geophysics*, 112, 268-278. <https://doi.org/10.1016/j.jappgeo.2014.11.017>

Ford, D.C., & Williams, P.W. (1989). *Karst geomorphology and hydrology*. London: Chapman & Hall.

Forte, E., & Pipan, M. (2017). Review of multi-offset GPR applications: data acquisition, processing and analysis. *Signal Processing*, 132, 210-220. <https://doi.org/10.1016/j.sigpro.2016.04.011>

Galagedara, L.W., Parkin, G.W., & Redman, J.D. (2003). An analysis of the ground-penetrating radar direct ground wave method for soil water content measurement. *Hydrological Processes*, 17, 3615–3628. <https://doi.org/10.1002/hyp.1351>

Garcia-Garcia, F., Valls-Ayuso, A., Benlloch-Marco, J., & Valcuende-Paya, M. (2017). An optimization of the work disruption by 3D cavity mapping using GPR: a new sewerage project in Torrente (Valencia, Spain). *Construction and Building Materials*, 154, 1226-1233. <https://doi.org/10.1016/j.conbuildmat.2017.06.116>

Graham Wall, B.R. (2006). Influence of depositional setting and sedimentary fabric on mechanical layer evolution in carbonate aquifers. *Sedimentary Geology*, 184, 203-224. <https://doi.org/10.1016/j.sedgeo.2005.11.003>

Grandjean, G., & Gourry, J.C. (1996). GPR data processing for 3D fracture mapping in a marble quarry (Thassos, Greece). *Journal of Applied Geophysics*, 36, 19-30. [https://doi.org/10.1016/S0926-9851\(96\)00029-8](https://doi.org/10.1016/S0926-9851(96)00029-8)

Green, J.A., Runkel, A.C., Alexander, E.C. Jr., (2012). Karst conduit flow in the Cambrian St. Lawrence formation, southeast Minnesota. *USA Carbonates Evaporites*, 27 (2), 167-172.

Grote, K., Anger, C., Kelly, B., Hubbard, S., & Rubin, Y. (2010). Characterization of soil water content variability and soil texture using GPR groundwave techniques. *Journal of Environmental and Engineering Geophysics*, 15, 93-110. <https://doi.org/10.2113/JEEG15.3.93>

Grote, K., Hubbard, S., & Rubin, Y. (2003). Field-scale estimation of volumetric water content using ground-penetrating radar ground wave techniques. *Water Resources Research*, 39, 1321. <https://doi.org/10.1029/2003WR002045>

Hamma, S.-Y., Kim, M., Cheong, J.-Y., Kim, J.-Y., Son, M., & Kim T.-W. (2007). Relationship between hydraulic conductivity and fracture properties estimated from packer tests and borehole data in a fractured granite. *Engineering Geology*, 92, 73-87. <https://doi.org/10.1016/j.enggeo.2007.03.010>

Hoek, E., & Bray, J.D. (1981). *Rock slope engineering* (3rd ed.). London: Taylor & Francis.
<https://doi.org/10.2113/12.2.125>

Huisman, J.A., & Bouten, W. (2003). Accuracy and reproducibility of measuring soil water content with the ground wave of ground penetrating radar. *Journal of Environmental and Engineering Geophysics*, 8, 65-73. <https://doi.org/10.4133/JEEG8.2.67>

Huisman, J.A., Hubbard, S.S., Redman, J.D., & Annan, A.P. (2003). Measuring soil water content with ground penetrating radar: a review. *Vadose Zone Journal*, 2, 476-491.
<https://doi.org/10.2136/vzj2003.4760>

Huisman, J.A., Snepvangers, J.J.J.C., Bouten, W., & Heuvelink, G.B.M. (2003). Monitoring temporal development of spatial soil water content variation: comparison of ground penetrating radar and time domain reflectometry. *Vadose Zone Journal*, 2, 519-529.
<https://doi.org/10.2136/vzj2003.5190>

Huisman, J.A., Sperl, C., Bouten, W., & Verstraten, J.M. (2001). Soil water content measurements at different scales: accuracy of time domain reflectometry and ground-penetrating radar. *Journal of Hydrology*, 245, 48-58. [https://doi.org/10.1016/S0022-1694\(01\)00336-5](https://doi.org/10.1016/S0022-1694(01)00336-5)

Klenk, P., Jaumann, S., & Roth, K. (2015). Monitoring infiltration processes with high-resolution surface-based ground-penetrating radar. *Hydrology Earth System Sciences Discussion*, 12, 12215-12246. <https://doi.org/10.5194/hessd-12-12215-2015>

Leckebusch, J. (2003). Ground-penetrating radar: a modern three-dimensional prospection method. *Archaeological Prospection*, 10, 213-240. <https://doi.org/10.1002/arp.211>

Longoni, L., Arosio, D., Scaioni, M., Papini, M., Zanzi, L., Roncella, R., & Brambilla, D. (2012). Surface and subsurface non-invasive investigations to improve the characterization of a fractured rock mass. *Journal of Geophysics and Engineering*, 9, 461-472.
<https://doi.org/10.1088/1742-2132/9/5/461>

Lunt, I.A., Hubbard, S.S., & Rubin Y. (2005). Soil moisture content estimation using ground-penetrating radar reflection data. *Journal of Hydrology*, 307, 254-269.
<https://doi.org/10.1016/j.jhydrol.2004.10.014>

Minet, J., Bogaert, P., Vanclooster, M., & Lambot, S. (2012). Validation of ground penetrating radar full-waveform inversion for field scale soil moisture mapping. *Journal of Hydrology*, 424-425, 112-123. <https://doi.org/10.1016/j.jhydrol.2011.12.034>

Nappi, M., Esposito, L., Piscopo, V., & Rega G. (2005). Hydraulic characterisation of some arenaceous rocks of Molise (Southern Italy) through outcropping measurements and Lugeon tests. *Engineering Geology*, 81, 54-64. <https://doi.org/10.1016/j.enggeo.2005.07.007>

Neal, A. (2004). Ground-penetrating radar and its use in sedimentology: principles, problems and progress. *Earth-Science Reviews*, 66, 261-330. <https://doi.org/10.1016/j.earscirev.2004.01.004>

Neto, P.X., & Medeiros, W.E. (2006). A practical approach to correct attenuation effects in GPR data. *Journal of Applied Geophysics*, 59, 140-151. <https://doi.org/10.1016/j.jappgeo.2005.09.002>

Pérez, V. (2001). *Radar del subsuelo. Evaluación en arqueología y en patrimonio histórico-artístico*. PhD thesis, Polytechnic University of Catalonia, Barcelona, Spain.

Pérez-Gracia, V., García García, F. & Rodríguez Abad, I. (2008). GPR evaluation of the damage found in the reinforced concrete base of a block of flats: A case study. *NDT & E International*, 41, 341-353. <https://doi.org/10.1016/j.ndteint.2008.01.001>

Pipan, M., Forte, E., Guangyou, F., & Finetti, I. (2003). High resolution GPR imaging and joint characterization in limestone. *Near Surface Geophysics*, 1, 39-55. <https://doi.org/10.3997/1873-0604.2002006>

Price, M., Robertson, A.S., & Foster, S.S.D. (1977). Chalk permeability - a study of vertical variation using water injection tests and borehole logging. *Water Services*, 81, 603-610.

Priest, S.D. (1993). *Discontinuity analysis for rock engineering* (1st ed.). London: Chapman & Hall.

Pueyo Anchuela, Ó., Casas-Sainz, A.M., Soriano, M.A., & Pocoví-Juan, A. (2009). Mapping subsurface karst features with GPR: results and limitations. *Environmental Geology*, 58, 391-399. <https://doi.org/10.1007/s00254-008-1603-7>

Rosell, J., & Cárcamo, J. (1994). *La fábrica de Ceres de Bilbao. Los orígenes del hormigón armado y su introducción en Bizkaia*. Bilbao: Colegio Oficial de Aparejadores y Arquitectos Técnicos de Bizkaia.

Runkel, A.C., Tipping, R.G., Alexander E.C. Jr., Green, J.A., Mossler J.H., Alexander, S.C. (2003). Hydrogeology of the Paleozoic bedrock in southeastern Minnesota. Minnesota Geological Survey Report of Investigation, 61, 105 pp, 1 map.

Runkel, A.C., Tipping, R.G., Alexander, E.C. Jr., Alexander, S.C. (2006). Hydrostratigraphic characterization of intergranular and secondary porosity in part of the Cambrian sandstone aquifer systems of the cratonic interior of North America: improving predictability of hydrogeologic properties. *Sedimentary Geology*, 184, 281-304. <https://doi.org/10.1016/j.sedgeo.2005.11.006>

Runkel, A.C., Tipping, R.G., Meyer, J.R., Steenberg, J.R., Retzler, A.J., Parker, B.L., Green, J.A., Barry, J.D., Jones, P.M. (2018). A multidisciplinary-based conceptual model of a fractured sedimentary bedrock aquitard: improved prediction of aquitard integrity. *Hydrological Journal*, 26, 2133-2159. <https://doi.org/10.1007/s10040-018-1794-2>

Sánchez, M.A., Foyo, A., & Tomillo, C. (2006). Application of the Lugeon test in landfill hydrologic studies. *Environmental and Engineering Geoscience*, 12, 125-136.

Schmalholz, J., Stoffregen, H., Kemna, A., & Yaramanci, U. (2004). Imaging of water content distributions inside a lysimeter using GPR tomography. *Vadose Zone Journal*, 3, 1106-1115. <https://doi.org/10.2113/3.4.1106>

Su, L.-J., Xu, X.-Q., Geng, X.-Y., & Liang, S.-Q. (2017). An integrated geophysical approach for investigating hydro-geological characteristics of a debris landslide in the Wenchuan earthquake area. *Engineering Geology*, 219, 52-63. <https://doi.org/10.1016/j.enggeo.2016.11.020>

Sudo, H., Tanaka, T., Kobayashi, T., Kondo, T., Takahashi, T., Miyamoto, M., & Amagai, M. (2004). Permeability imaging in granitic rocks based on surface resistivity profiling. *Exploration Geophysics*, 35, 56-61. <https://doi.org/10.1071/EG04056>

Trinks, I., Wachsmuth, D., & Stümpel, H. (2001). Monitoring water flow in the unsaturated zone using georadar, *First Break*, 19, 679-684. <https://doi.org/10.1046/j.1365-2397.2001.00228.x>

Turesson, A. (2006). Water content and porosity estimated from ground-penetrating radar and resistivity. *Journal of Applied Geophysics*, 58, 99-111. <https://doi.org/10.1016/j.jappgeo.2005.04.004>

Van Overmeeren, R.A. (1994). Georadar for hydrogeology. *First Break*, 12, 401-408. <https://doi.org/10.3997/1365-2397.1994025>

Van Overmeeren, R.A., Sariowan, S.V., & Gehrels J.C. (1997). Ground penetrating radar for determining volumetric soil water content; results of comparative measurements at two test sites. *Journal of Hydrology*, 197, 316-338. [https://doi.org/10.1016/S0022-1694\(96\)03244-1](https://doi.org/10.1016/S0022-1694(96)03244-1)

Weihermüller, L., Huisman, J.A., Lambot, S., Herbst, M., & Vereecken, H. (2007). Mapping the spatial variation of soil water content at the field scale with different ground penetrating radar techniques. *Journal of Hydrology*, 340, 205-216. <https://doi.org/10.1016/j.jhydrol.2007.04.013>

Weiler, K.W., Steenhuis, T.S., Boll, J., & Kung, K-J.S. (1998). Comparison of ground penetrating radar and time-domain reflectometry as soil water sensors. *Soil Science Society of America Journal*, 62, 1237-1239. <https://doi.org/10.2136/sssaj1998.03615995006200050013x>

Worthington, S.R.H. (2015). Diagnostic test for conceptualizing transport in bedrock aquifers. *Journal of Hydrology*, 529, 365-372. <https://dx.doi.org/10.1016/j.jhydrol.2015.08.002>

Table 1. Main fracture sets characteristics

Fracture set	Dip (°)		Dip direction (°)		Spacing (m)		Aperture (mm)
	Mean	Std deviation	Mean	Std deviation	Mean	Std deviation	
	B _p	89	2	212	5	0.32	
J ₁	22	6	299	9	0.41	0.07	0.50-2.50
J ₂	82	2	133	7	0.60	0.1	0.10-0.25

Accepted Article

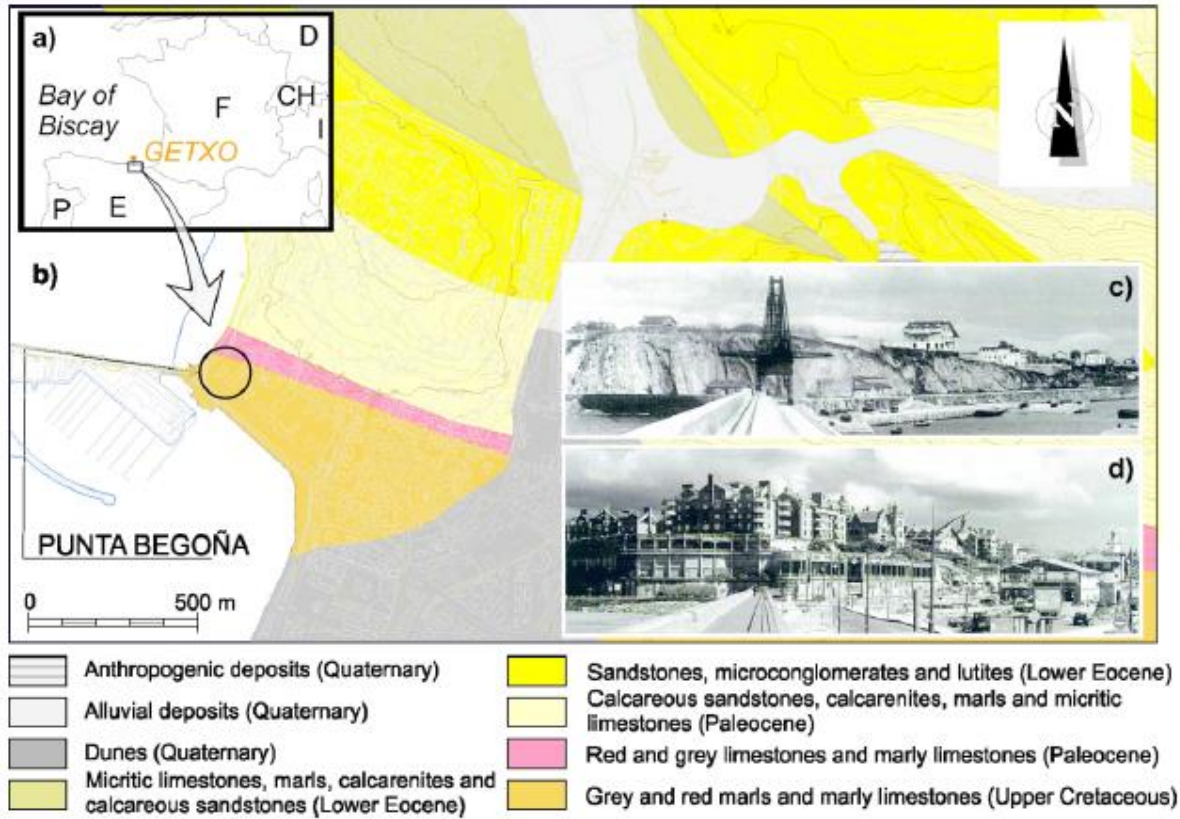


Fig. 1. (a) Geographical location of the study site: Punta Begoña Galleries (Getxo, Basque Country, Spain). (b) Geological and hydrogeological context. (c) Image of the cliff prior to the construction of Punta Begoña Galleries. (d) Present view of the Punta Begoña Galleries.

Accepte



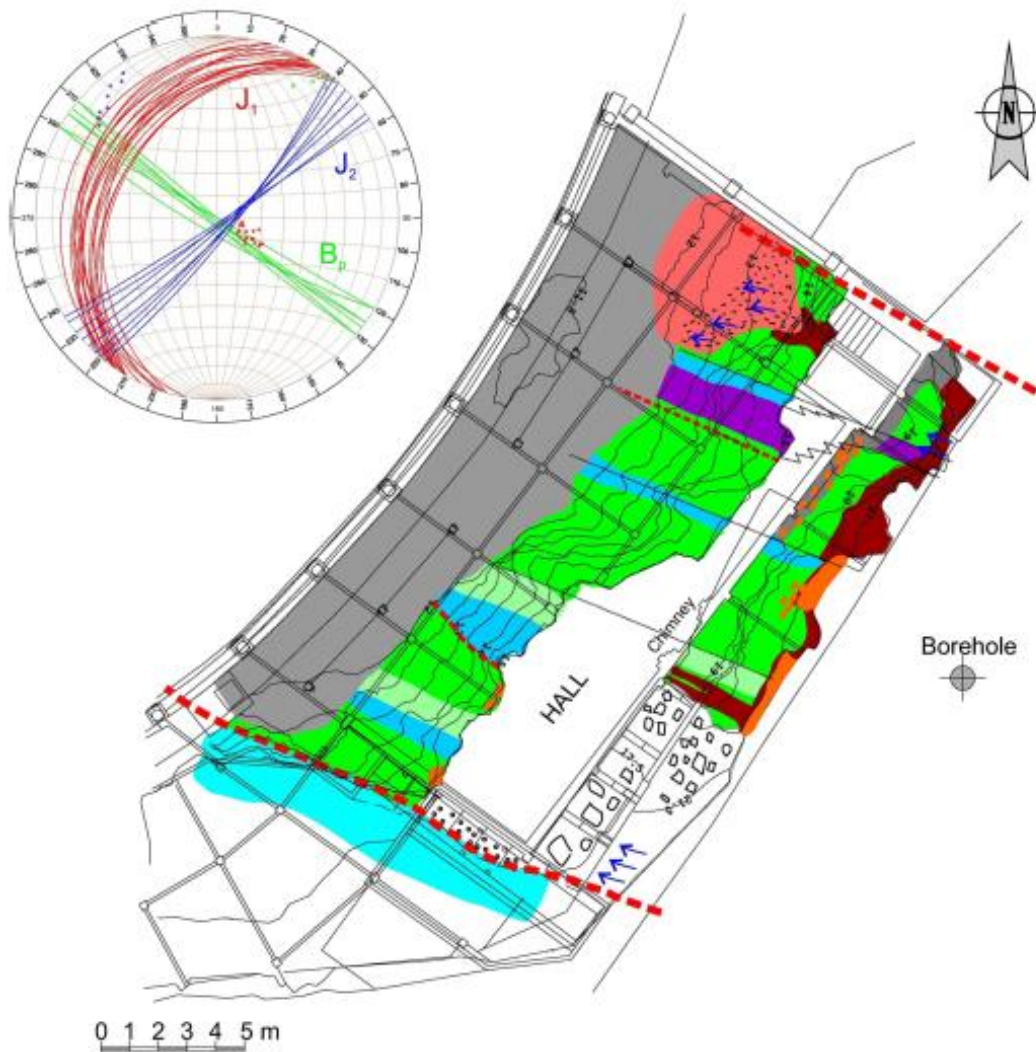
Fig. 2. Three-dimensional image of the investigated area. Photograph of the building hall, main built body, damaged not only by water inflows from the roof but also by underground flows coming from the upper terrace.

Accepted Article



Fig. 3. Plan of the galleries. Location of the GPR profiles (blue lines).

Accepte



LEGEND


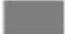








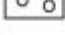

	Marls		Anthropogenic deposits		Fillers and wet soils
	Layered marls		Rubble		Soil from marls degradation
	Reddish marls		Wall building sandstones		Fault plane
	Marly limestones		Fillers in the area under stairs		Water inlet flow

Fig. 4. Detailed geological cartography of the hall surroundings and a stereographic projection of the main fracture sets. The orange/brown zones mark wet and/or altered rock areas mainly affected by water.

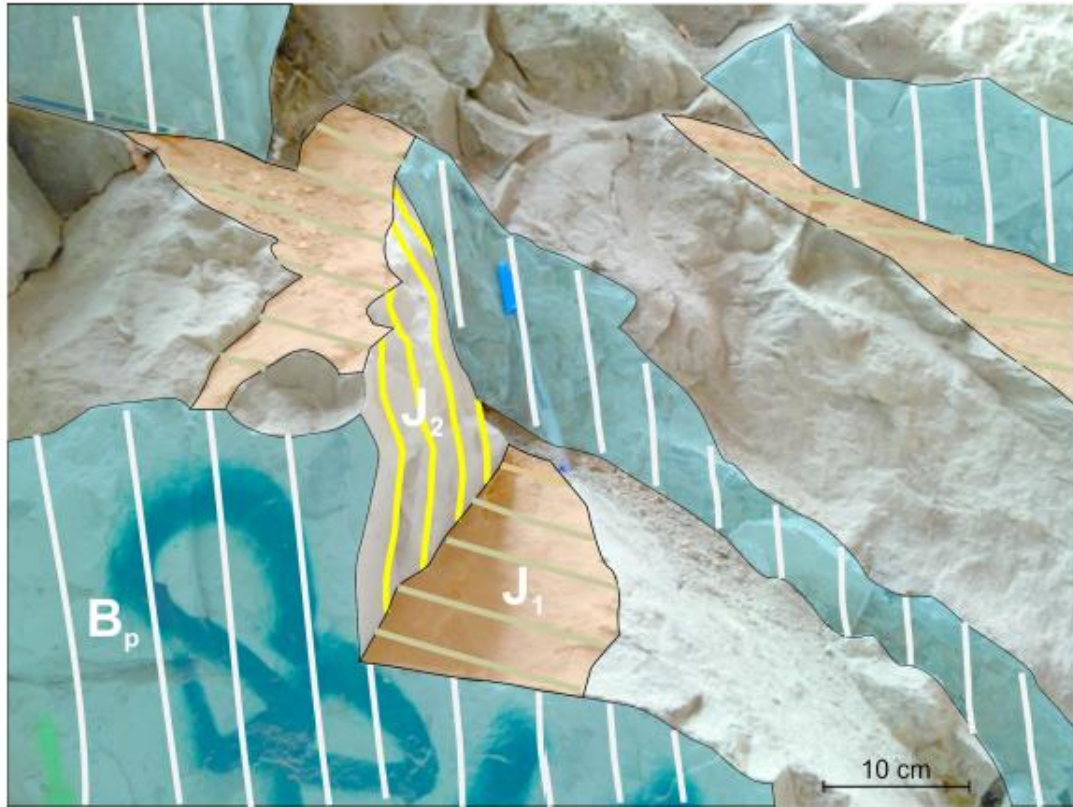


Fig. 5. Detailed view of the 3 main fracture sets (B_p, J₁ and J₂) present in the cliff.

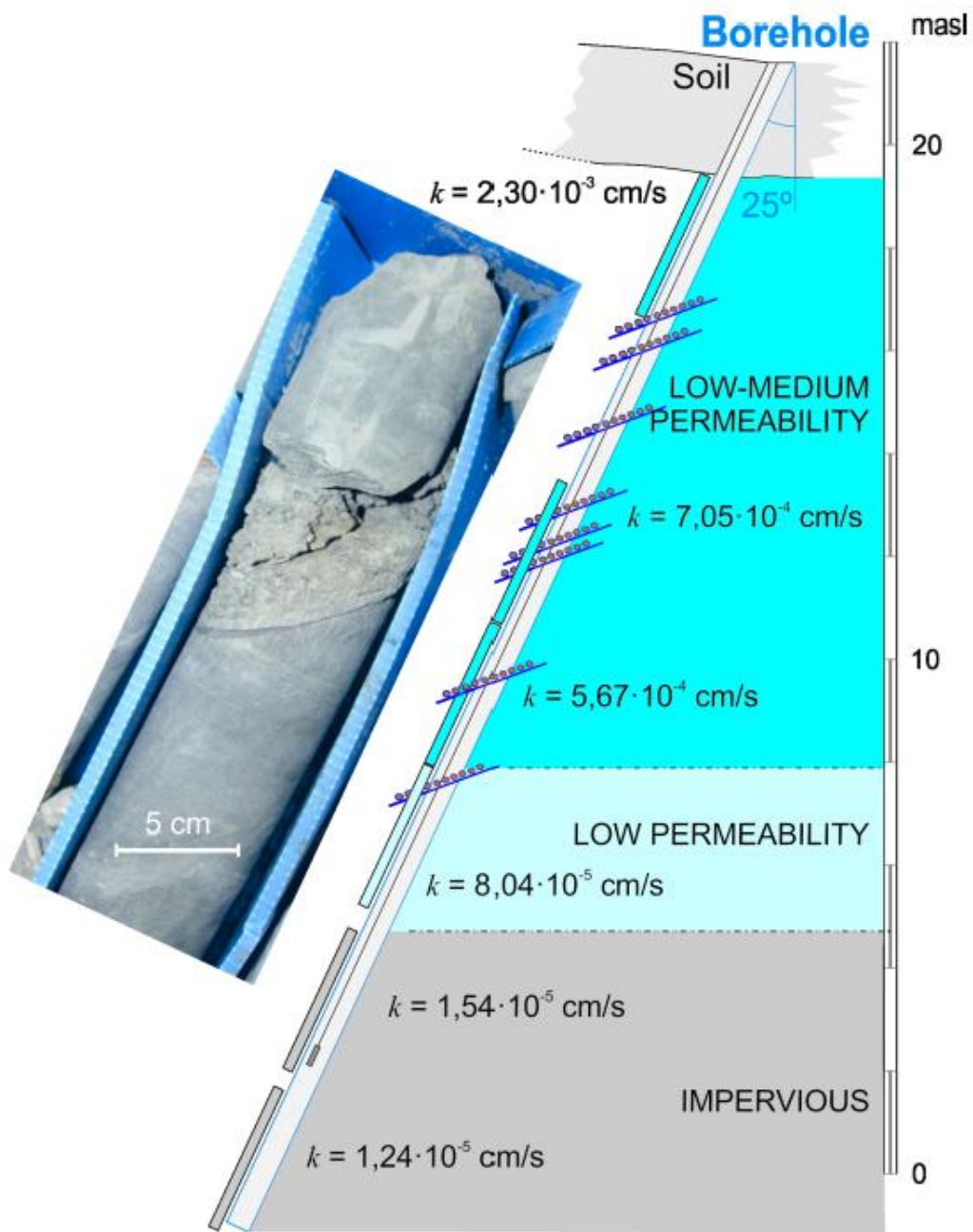


Fig. 6. Massif permeability along the borehole. Core sample fragment where the open joint J1 was observed with remains of oriented pebbles marking preferential flows.

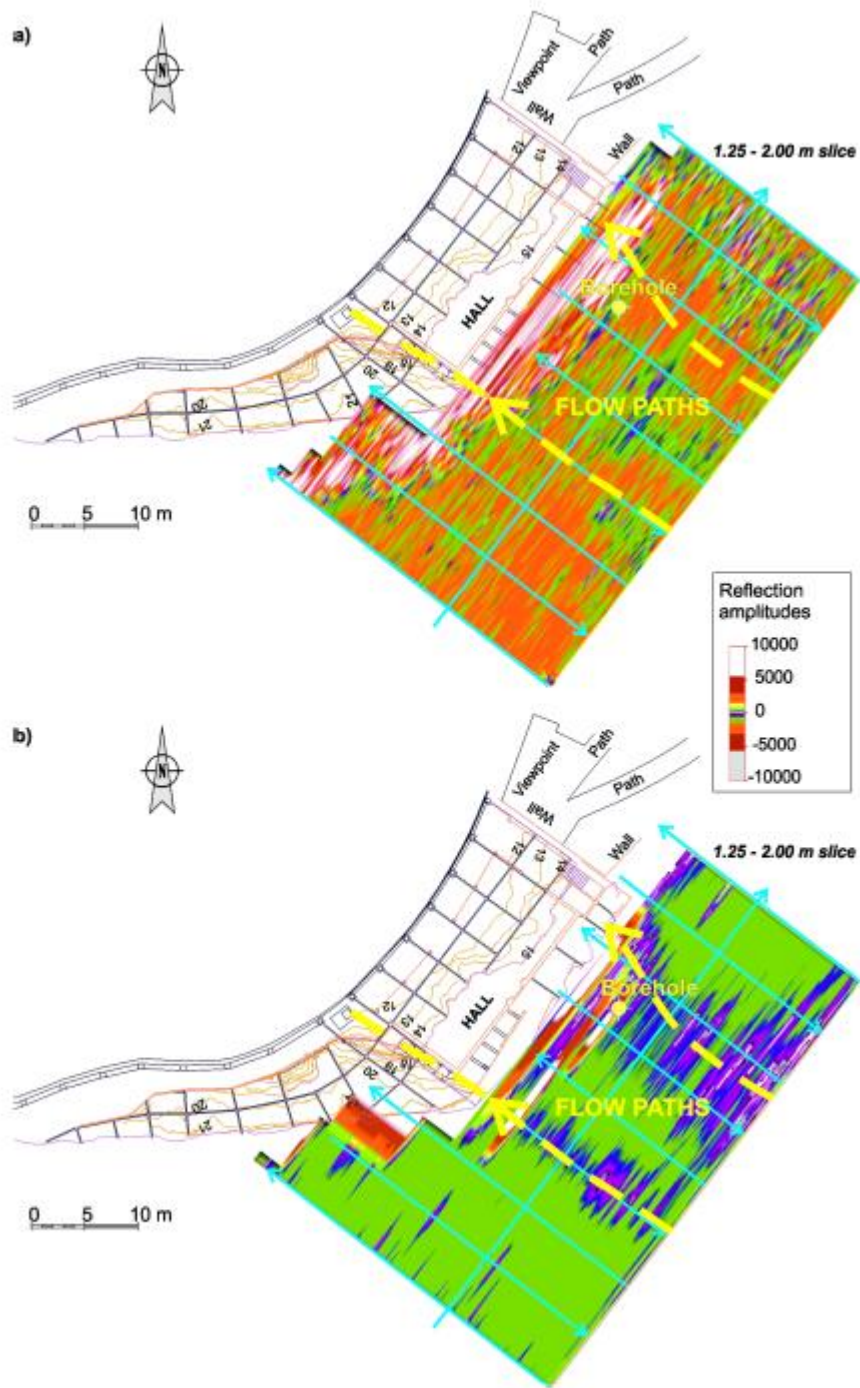


Fig. 7. Amplitude maps of the 1.75-2.00 m slice of the upper terrace where the detected flow paths are shown. Data collected with 400 MHz during 2 well-differentiated hydrodynamic period: a rainy period (a) and the driest season (b).

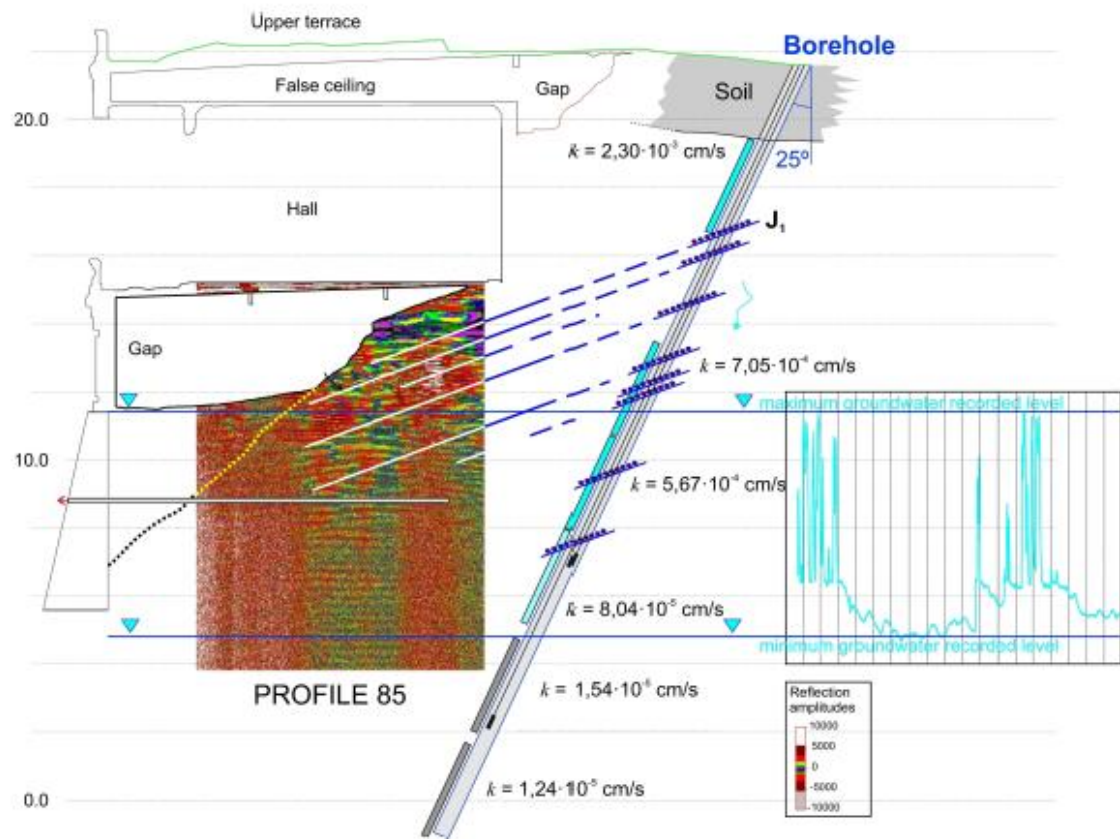


Fig. 8. Radargram of profile 85 mounted on the hall topography and interpreted according to the hydrogeological information.

Accepted

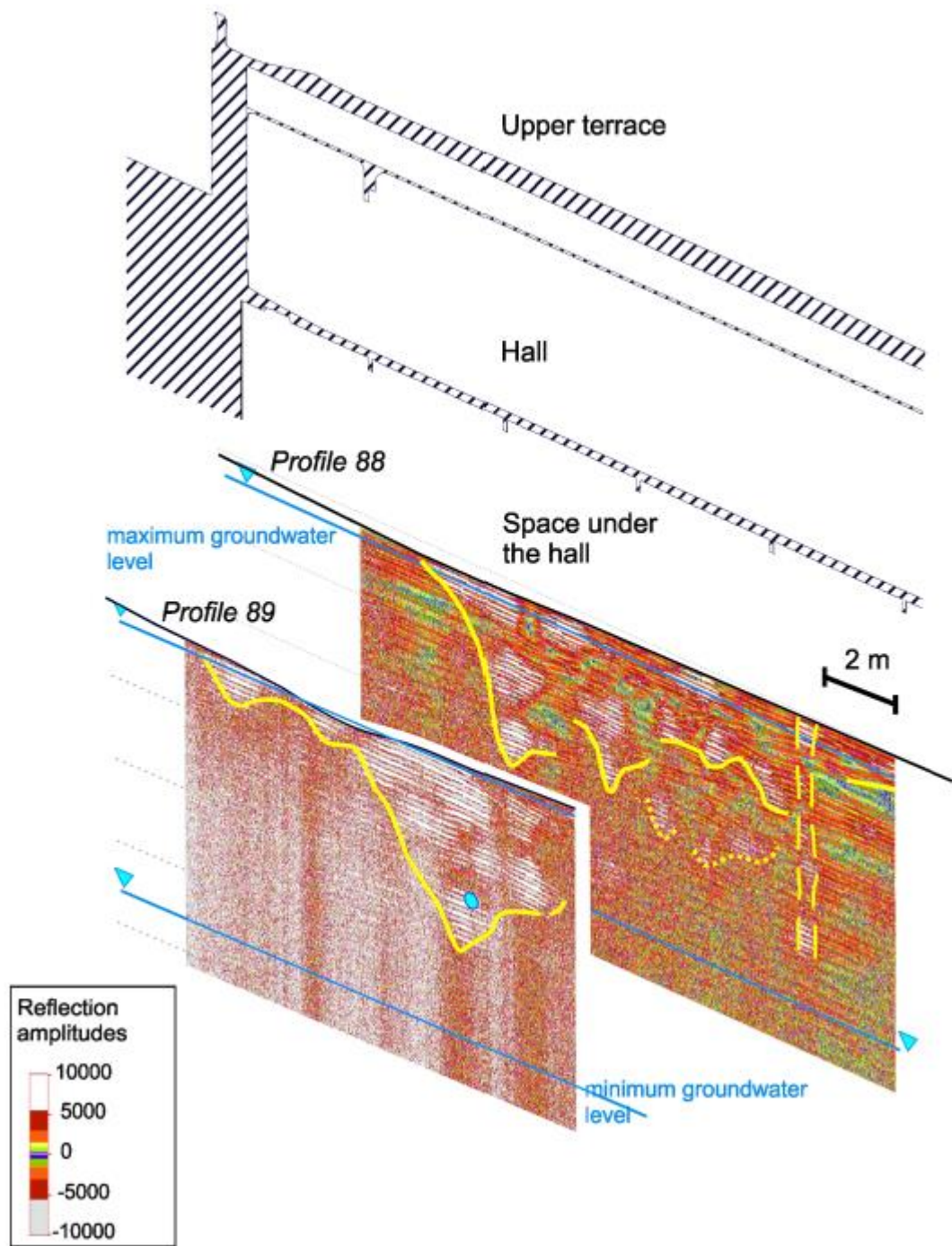


Fig. 9. Radargrams of profiles 88 and 89 showing a clear change that was identifiable as the original cliff relief.

Article title: Characterization of complex groundwater flows in the environment of singular buildings by combining hydrogeological and non-destructive geophysical (ground-penetrating radar) techniques: Punta Begoña Galleries (Getxo, Spain)

Authors' name: Jesus A. URIARTE, Laura DAMAS MOLLÁ, Maialen SAGARNA, Arantza ARANBURU, Francisco GARCÍA, Iñaki ANTIGÜEDAD, Tomás MORALES*

Summary:

The use of non-destructive GPR techniques in dry and wet periods, combined with injection tests, allows characterization of complex underground flows in built-up areas.

Results provide detailed information on flow dynamics with respect to their restoration.

This approach is particularly recommended in sites of high heritage value in which respectful and minimal invasive interventions are advised.

Figure:

